Journal of Civil Structural Health Monitoring
https://doi.org/10.1007/s13349-023-00693-6

ORIGINAL PAPER

Influence of system changes on closely spaced modes of a large-scale concrete tower for the application to structural health monitoring

Clemens Jonscher[1] · Leon Liesecke[1] · Nikolai Penner[1] · Benedikt Hofmeister[1] · Tanja Grießmann[1] · Raimund Rolfes[1]

Received: 19 December 2022 / Accepted: 30 March 2023

Abstract
Concrete steel towers are increasingly being used for onshore wind turbines. The lower part consists of separated segmented concrete rings connected with dry joints. Due to slight deviations from the axisymmetric cross-section, closely spaced modes occur. Therefore, the influences of small system changes on closely spaced modes, particularly the mode shapes, should be investigated to enable reliable vibration-based monitoring. In this context, the influence of imperfections due to the waviness of the dry joints requires attention. As no acceleration measurements on concrete towers considering small system changes have been performed so far, this has not yet been investigated. Therefore, an experiment is carried out using a large-scale laboratory model of a prestressed concrete segment tower. The system modifications are introduced by changing the preload. This changes the influence of imperfections of the surfaces of the horizontal dry joints, estimated by measuring strain and displacement at the lowest joint. An increasing preload causes the first two pairs of bending modes to move closer together. This enables to study the effect of the closeness of natural frequencies on the related mode shapes based on the same structure. Thus, the known effects of increasing uncertainty of the alignment and a rotation of the mode shape in the mode subspace with closer natural frequencies can be shown experimentally. In this work, the operational modal analysis (OMA) methods Bayesian-OMA (BAYOMA) and Stochastic Subspace Identification (SSI) are used. Local imperfections can significantly affect modal parameters, so these should be considered for vibration-based monitoring.

Keywords Close modes · Concrete steel tower · OMA · Identification uncertainty

1 Introduction

In the construction of wind turbines, the tower is a decisive cost factor due to material and transport costs. With increasing tower heights, hybrid towers are often used for onshore wind turbines. This type of tower, as shown in Fig. 1, consists of segmented concrete rings with vertical and horizontal dry joints in the lower part and conical steel tubes in the upper part. They reach hub heights of over 160 m [6] and can be particularly economical due to lower transport as well as manufacturing costs compared to conventional steel towers. The increase in economic efficiency is achieved by prefabricating the lower tower section in segments and providing the structural integrity by externally prestressing the concrete after stacking the segment rings.

In a segmented concrete tower, geometric and material nonlinearities occur due to the contact at the horizontal dry joints. Due to the manufacturing process, the contact surface exhibits imperfections in the form of waviness, as shown in Fig. 1. The waviness leads to an uneven load distribution between segment rings on a local level. Hence, an inhomogeneous stress distribution emerges at the joint, as Theiler et al. [28] demonstrated numerically. In a large-scale laboratory experiment of a prestressed segmented concrete tower,

✉ Clemens Jonscher
c.jonscher@isd.uni-hannover.de

Leon Liesecke
l.liesecke@isd.uni-hannover.de

Nikolai Penner
n.penner@isd.uni-hannover.de

Benedikt Hofmeister
b.hofmeister@isd.uni-hannover.de

Tanja Grießmann
t.griessmann@isd.uni-hannover.de

Raimund Rolfes
r.rolfes@isd.uni-hannover.de

[1] Institute of Structural Analysis, Leibniz Universität Hannover, Appelstraße 9A, 30163 Hanover, Germany

Published online: 13 April 2023

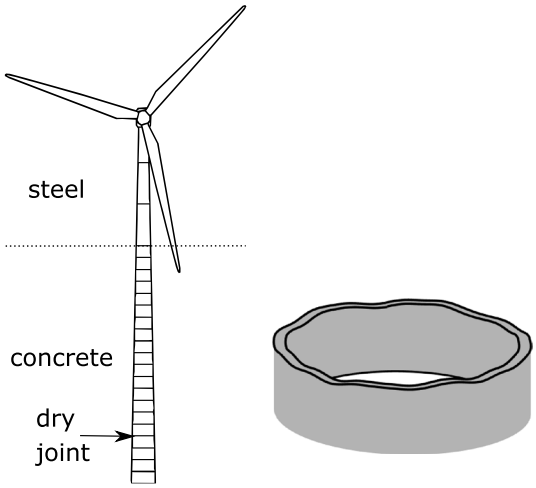

Fig. 1 Right: Sketch of a wind turbine with a hybrid tower similar to [23]. Left: Illustration of the imperfection due to waviness of a dry horizontal joint

the inhomogeneous strain distribution was detected using displacement and strain measurements at the joint [23]. The experiments showed that while the mean value of the strain distribution at the joint increases with the preload, the inhomogeneous strain distribution remained qualitatively the same under varying preload.

An early damage detection for the segment joints can be achieved using a structural health monitoring (SHM) approach. A distinction can be made between local and global monitoring. In the case of local monitoring, measurements are taken in the area of an expected damage location—for example, concrete spalling at the dry joint. Strain gauges are often used for this purpose. In contrast to this, global monitoring, like vibration-based, attempts to obtain a statement about the global state of the monitored structure on the basis of fewer sensors [16]. This makes global monitoring significantly more cost-effective. However, measurements are more difficult to interpret and usually damages as small as with local monitoring cannot be identified. For a global vibration-based monitoring concept of a hybrid tower, knowledge of the influence of imperfections on the modal parameters is necessary.

For vibration-based global monitoring, operational modal analysis (OMA) identification methods are mostly used, as they do not require equipping the monitored structure with additional excitation actuators like e.g. electromagnetic shakers. A challenge that arises when monitoring a tower structure with a symmetrical cross-section is the identification of closely spaced bending modes. The widely used frequency domain decomposition (FDD) method determines the modal parameters from the singular value decomposition (SVD) of the spectral matrix [10]. Hence, the FDD can only approximately identify the modal parameters in the case of closely spaced modes, because the excitation can usually not be modally decoupled. An alternative frequency domain identification method is the Bayesian operational modal analysis (BAYOMA), which is able to properly identify closely spaced modes [3]. In addition, this method also provides the uncertainty of modal parameters. A more detailed investigation of the identification uncertainty of closely spaced modes when using BAYOMA demonstrates, that mode shapes in particular are more uncertain to identify than in a well separated case [4]. However, in case of a high signal to noise ratio (SNR), the identification of the mode subspace (MSS) is still possible with a low uncertainty. A detailed description of the BAYOMA method is given in Sect. 2.

In time domain, the stochastic subspace identification (SSI) [29] is a popular OMA method. A distinction can be made between covariance-driven (SSI-COV) and data-driven stochastic subspace identification (SSI-DAT). In SSI-DAT, the raw data is used as the basis for the system identification, whereas in SSI-COV, covariance matrices are used. For both methods, it is a challenge to distinguish physical modes from spurious modes and to find stable paths with respect to the model order. So-called stabilisation diagrams and various additional algorithms are used for the mode selection, with some of these being able to identify closely spaced modes [18, 26].

In addition to the methods mentioned above, there are further OMA algorithms that can identify closely spaced modes, like natural excitation technique with eigensystem realisation (NExT ERA) [19] and poly-reference least squares complex frequency-domain (pLSCF) [24].

In the literature, there are several examples of experimental investigations of the dynamics of structures with closely spaced modes. For instance, a prototype of a concrete tower of a wind turbine was investigated [12]. In that study, the cross-section was symmetrical, however, the bending modes were well-separated due to attachments mounted to the structure. Similar results were shown in a study of a monopole telecoms structure [20], where the expected alignment of the first mode shape due to physical attachments also corresponds to the identified alignment. Brownjohn et al. [11] investigated the dynamics of offshore lighthouses using BAYOMA and also found a significant difference in the bending mode natural frequencies, which are also due to attachments. However, by taking into account the uncertainties of the mode shapes, the alignment of the mode shapes was not necessarily the same as the visible structural symmetry. The influence of environmental conditions and damage on closely spaced modes was investigated using the Leibniz University Test Structure for Monitoring (LUMO) considering the identification uncertainties [22]. In this study, the comparison of mode shapes with a mode subspace proved to be much more reliable than a simple comparison of mode

shapes and thus a better damage-sensitive feature for closely spaced modes. Dooms et al. examined a silo using the SSI and found out that in case of closely spaced modes, complex mode shapes occur that have no dominant phase in the complex plane [15]. A similar observation was made when examining a steel mast [27].

In this work, the investigations of the influence of small system changes on modal parameters, in particular on the mode alignment, of closely spaced modes are carried out on a large scaled prestressed concrete tower with horizontal dry joints in a laboratory. This makes it possible to selectively insert system changes, such as changes of the preload. At the same time, undesirable influences, such as temperature changes and operational conditions, can be largely avoided. Due to the symmetrical tower structure closely spaced modes occur, which can be influenced by system changes. As OMA methods do not require measurements of the excitation, they are suitable for many real-world applications, like vibration-based monitoring of tower structures. Therefore, OMA methods are used in this case study. The excitation in the experiment originates from the ambient influences from the laboratory and is not measured.

BAYOMA is used as the identification method, since an uncertainty calculation can be carried out. This allows a more precise investigation of closely spaced modes and the influence of smallest system changes. To verify that the effects to be observed are not caused by the identification method, the results are compared with the SSI-COV. In order to be able to estimate the changes in the imperfections due to the change of the preload, local monitoring of the lowest joint is also performed on the basis of strain and displacement measurements. In the following chapter, the two identification methods are described in more detail and the special characteristics of closely spaced modes are discussed. Chapter 3 describes the experiment and the results are presented in Chapter 4. Afterwards, the study will be summarised and an outlook will be given.

2 Operational modal analysis

For vibration-based monitoring of large structures, OMA is usually employed. Unlike experimental modal analysis, the excitation is unknown [9]. Instead, it is assumed that the structure is excited with a distributed stochastic force $\boldsymbol{f}$, which exhibits a white noise spectrum in the considered frequency range. The structural responses (displacements $\boldsymbol{u}$, velocities $\dot{\boldsymbol{u}}$ and accelerations $\ddot{\boldsymbol{u}}$) of a linear time invariant mechanical structure to such a force are expressed using the equation of motion for a n degree-of-freedom (DOF) system

$$\boldsymbol{M}\ddot{\boldsymbol{u}} + \boldsymbol{C}\dot{\boldsymbol{u}} + \boldsymbol{K}\boldsymbol{u} = \boldsymbol{f}, \tag{1}$$

with $\boldsymbol{M}$, $\boldsymbol{C}$ and $\boldsymbol{K}$ as mass -, damping- and stiffness matrices. For the case of modal damping, the system can be modally decoupled with $\boldsymbol{u} = \boldsymbol{\Phi}\boldsymbol{q}$, where $\boldsymbol{\Phi}$ is the modal matrix, that contains n mode shape vectors $\boldsymbol{\Phi} = [\boldsymbol{\varphi}_1 ... \boldsymbol{\varphi}_n]$ and the modal coordinate vector $\boldsymbol{q}$. The decoupled equation of motion for each mode corresponds to that of a single DOF system

$$\ddot{q}_j + 4\zeta_j \pi f_{0j} \dot{q}_j + 4\pi^2 f_{0j}^2 q_j = p_j, \tag{2}$$

where p_j is the modal force, ζ_j is the modal damping and f_{0j} the natural frequency of the system. BAYOMA uses modal decoupling, which is described in the following subsection. In contrast, the SSI-COV identifies a state space model for the system. This method will be briefly explained in subsection 2.2.

2.1 Bayesian operational modal analysis

The basic idea of BAYOMA was introduced by Yuen et al. [31]. The method has been improved by Au et al. [2, 3] by reducing the number of design variables of the underlying numerical optimisation problem in case of many measurement degrees of freedom or closely spaced modes. In this chapter, an insight into the method is given. More information can be found in the corresponding literature e.g. [5].

The scaled discrete Fourier transformation (DFT) $\boldsymbol{\mathcal{F}}$ of a measured Gaussian distributed acceleration signal $\ddot{\boldsymbol{u}}$ with n_{Channel} channels, N_{data} data points and a sampling rate f_s with the corresponding frequency point $f_k = kf_s/N_{\text{data}}$ is

$$\boldsymbol{\mathcal{F}}_k = \boldsymbol{\mathcal{F}}(f_k) = \sqrt{\frac{1}{N_{\text{data}} f_s}} \sum_{j=0}^{N_{\text{data}}-1} \ddot{\boldsymbol{u}}_j e^{-2\pi i j k / N_{\text{data}}}, \tag{3}$$

where i is the imaginary number. In case of a high sampling rate and a long data duration, the DFT is asymptotically independent and Gaussian distributed at different frequencies. In the case of N_{modes} dominant modes in the considered frequency range, the model of the DFT is

$$\boldsymbol{\mathcal{F}}_k = \sum_{j=1}^{N_{\text{modes}}} \boldsymbol{\varphi}_j h_{jk} s_{jk} + \boldsymbol{\epsilon}_k \text{ with } h_{jk} = \frac{-1}{1 - \beta_{jk}^2 - 2\beta_{jk}\zeta_j i} \text{ and } \beta_{jk} = \frac{f_{0j}}{f_k}, \tag{4}$$

where $\boldsymbol{\varphi}_j$ is the unit norm mode shape vector, s_{jk} is the modal force in the frequency domain, $\boldsymbol{\epsilon}_k$ is the modelling error and h_{jk} is the transfer function of a damped 1-DOF system for acceleration responses. The assumption that the power spectral density (PSD) of the modelling error is equal for all channels and has the constant value S_e in the considered frequency range leads to $E[\boldsymbol{\epsilon}_k \boldsymbol{\epsilon}_k^* | \boldsymbol{\Theta}] = S_e \boldsymbol{I}_{n_{\text{Channel}}}$, where $\boldsymbol{I}_{n_{\text{Channel}}}$ is the n_{Channel} x n_{Channel} unity matrix. In addition, it is assumed, that the hermitian PSD matrix of the modal force $\boldsymbol{S}$ is constant in the considered frequency range and independent of the modelling error, the expected value of the PSD is

$$\boldsymbol{E}_k(\Theta) = E[\boldsymbol{\mathcal{F}}_k\boldsymbol{\mathcal{F}}_k^*|\boldsymbol{\Theta}] = \sum_{j=1}^{N_{\text{modes}}}\sum_{m=1}^{N_{\text{modes}}} h_{jk}h_{mk}^* S_{jm}\boldsymbol{\varphi}_j\boldsymbol{\varphi}_m^T + S_e\boldsymbol{I}_{n_{\text{Channel}}} = \boldsymbol{\Phi}\boldsymbol{H}_k\boldsymbol{\Phi}^T + S_e\boldsymbol{I}_{n_{\text{Channel}}}$$
$$\text{with } \boldsymbol{H}_k = \text{diag}([h_{1,k}\ldots h_{N_{\text{modes}},k}])\,\boldsymbol{S}\,\text{diag}([h_{1,k}\ldots h_{N_{\text{modes}},k}])^*. \tag{5}$$

Thus, $\boldsymbol{E}_k(\boldsymbol{\Theta})$ corresponds to the theoretical PSD of the modal parameters $\boldsymbol{\Theta}$ and corresponds to the covariance matrix of $\boldsymbol{\mathcal{F}}_k$. For two dominant modes, Eq. 5 is dependent on $9 + 2n_{\text{Channel}}$ parameters

$$\boldsymbol{\Theta} = [\boldsymbol{\varphi}_1^T, \boldsymbol{\varphi}_2^T, f_{01}, f_{02}, \zeta_1, \zeta_2, S_{11}, S_{22}, \text{Re}(S_{12}), \text{Im}(S_{12}), S_e]. \tag{6}$$

In the special case of incoherence of the modal force, the modal force matrix S is a diagonal matrix, so that the modes can be perfectly decoupled. In this case, extensions of the FDD could also identify the closely spaced modes without a bias. Applying the special case of Bayes' theorem, where the prior of the modal parameters is uniformly distributed, results in the posterior being proportional to the likelihood.

The negative loglikelihood function (NLLF) L for a multivariate Gaussian distribution is

$$L(\boldsymbol{\Theta}) = n_{\text{Channel}}N_f \ln\pi + \sum_{k=1}^{N_f}\ln\left|\boldsymbol{E}_k(\boldsymbol{\Theta})\right| + \sum_{k=1}^{N_f}\boldsymbol{\mathcal{F}}_k^*\boldsymbol{E}_k(\boldsymbol{\Theta})^{-1}\boldsymbol{\mathcal{F}}_k, \tag{7}$$

where N_f is the number of considered frequency points. The most probable values (MPV) of the modal parameters can then be obtained by minimising the NLLF and, therefore, solving for Θ.

With an increasing number of sensors, the number of parameters to be identified increases according to Eq. 6. To make the number of design parameters independent of the number of sensors, the mode shape subspace (MSS) is determined before starting the optimisation. The MSS is a subspace spanned by the m dominating mode shapes. To obtain the dominating mode shapes for the MSS the real part of the spectral matrix can be summed up over the frequency range of interest, assuming that the mode shape is real-valued

$$\boldsymbol{D} = \sum_{k=1}^{N_f}\text{Re}(\boldsymbol{\mathcal{F}}_k\boldsymbol{\mathcal{F}}_k^*). \tag{8}$$

The dominating mode shapes can be obtained by an eigenvalue decomposition. In the case of two modes, the MSS $\boldsymbol{\Psi}_{1,2}$ is determined from the unit norm eigenvectors $\boldsymbol{\Psi}$ of the two highest eigenvalues. The subsequent optimisation only needs to determine the rotation angle α_1 and α_2 of the modes in the MSS to obtain the mode shapes $\boldsymbol{\Phi} = \boldsymbol{\Psi}_{1,2}\boldsymbol{T}(\alpha_1, \alpha_2)$ using the transformation matrix $\boldsymbol{T}$

$$\boldsymbol{T}(\alpha_1, \alpha_2) = \begin{bmatrix}\cos(\alpha_1) & \cos(\alpha_2)\\ \sin(\alpha_1) & \sin(\alpha_2)\end{bmatrix}. \tag{9}$$

This converts the expected value of Eq. 5 into

$$\boldsymbol{E}_k(\boldsymbol{\Theta}_\alpha) = \boldsymbol{\Psi}_{1,2}\boldsymbol{T}\boldsymbol{H}_k(\boldsymbol{\Psi}_{1,2}\boldsymbol{T})^T + S_e\boldsymbol{\Psi}\boldsymbol{I}_n\boldsymbol{\Psi}^T,$$

with $\boldsymbol{\Theta}_\alpha = [\alpha_1, \alpha_2, f_{01}, f_{02}, \zeta_1, \zeta_2, S_{11}, S_{22}, \text{Re}(S_{12}), \text{Im}(S_{21}), S_e]$ Due to the transformation matrix, the unit length constraint is satisfied. Thus, 11 parameters are to be identified regardless of the number of sensors. Note that the mode shapes are not necessarily orthogonal due to the chosen sensor positions and measuring directions. An efficient way of solving this optimisation problem, as well as adjusting the mode subspace for very noisy data, can be found in [3].

Given the assumed Gaussian distribution, the posterior covariance of the modal parameters is calculated from the inverse Hessian matrix of the NLLF (Eq. 7) with the excepted value of Eq. 5 at the MPV. The mode shapes are constrained to unit norm in BAYOMA. The consideration of this constraint in the derivation, as well as the possibility of the numerical and analytical double derivation, is described in [2]. The roots of the diagonal entries are the standard deviation of the corresponding modal parameters.

2.2 Covariance-driven stochastic subspace identification

In the stochastic subspace identification, the system is modelled as a linear time-invariant discrete-time stochastic state space model

$$\begin{aligned}\boldsymbol{x}_{k+1} &= \boldsymbol{A}\boldsymbol{x}_k + \boldsymbol{w}_k\\ \boldsymbol{y}_k &= \boldsymbol{C}\boldsymbol{x}_k + \boldsymbol{v}_k\end{aligned} \tag{10}$$

with the state matrix $\boldsymbol{A}$, the output matrix $\boldsymbol{C}$, the discrete-time state vector $\boldsymbol{x}_k$ and the discrete-time output vector $\boldsymbol{y}_k$ [7]. The unknown input is modelled by the process noise $\boldsymbol{w}_k$ and the measurement noise $\boldsymbol{v}_k$. Both are assumed to be zero mean, uncorrelated and possessing a white noise power spectral density.

The modal parameters are calculated from the state matrix $\boldsymbol{A}$ and the output matrix $\boldsymbol{C}$. This is accomplished by determining the eigenvalues μ_i and eigenvectors $\boldsymbol{\theta}_i$ of $\boldsymbol{A}$ and deriving the continuous-time eigenvalues λ_i using $\lambda_i = \ln(\mu_i)f_s$.

The modal parameters, i.e. the natural frequencies f_i, damping ratios ζ_i and mode shapes $\boldsymbol{\varphi}_i$, can then be obtained with

$$f_i = \frac{|\lambda_i|}{2\pi},\ \zeta_i = \frac{-\mathrm{Re}(\lambda_i)}{|\lambda_i|},\ \boldsymbol{\varphi}_i = \boldsymbol{C}\theta_i. \tag{11}$$

The various SSI algorithms are classified in the literature as covariance-driven SSI or data-driven SSI [9]. The main difference between these approaches is the formulation of the subspace matrix $\boldsymbol{\mathcal{H}}$, from which the observability matrix $\mathcal{O}$ can be obtained. In this study, the SSI-COV is used for the system identification. In that case, the matrix $\boldsymbol{\mathcal{H}}$ with l block rows and m block columns is assembled from the covariance matrices $R_y(i)$

$$\boldsymbol{\mathcal{H}} = \begin{bmatrix} R_y(1) & R_y(2) & \dots & R_y(m) \\ R_y(2) & R_y(3) & \dots & R_y(m+1) \\ \vdots & \vdots & \ddots & \vdots \\ R_y(l) & R_y(l+1) & \dots & R_y(l+m-1) \end{bmatrix}. \tag{12}$$

The subspace matrix $\boldsymbol{\mathcal{H}}$ can be expressed as the matrix product $\boldsymbol{\mathcal{H}} = \boldsymbol{\mathcal{O}}\boldsymbol{\mathcal{Z}}$, using the observability matrix $\boldsymbol{\mathcal{O}}$ and a matrix $\boldsymbol{\mathcal{Z}}$. The observability matrix is defined as

$$\boldsymbol{\mathcal{O}} = \begin{bmatrix} \boldsymbol{C} \\ \boldsymbol{CA} \\ \dots \\ \boldsymbol{CA}^{l-1} \end{bmatrix}. \tag{13}$$

A singular value decomposition (SVD) is used to obtain $\boldsymbol{\mathcal{H}} = \boldsymbol{USV}^T$, which enables solving for the matrices $\boldsymbol{\mathcal{O}}$ and $\boldsymbol{\mathcal{Z}}$

$$\boldsymbol{\mathcal{O}} = \boldsymbol{US}^{1/2} \text{ and } \boldsymbol{\mathcal{Z}} = \boldsymbol{S}^{1/2}\boldsymbol{V}^T. \tag{14}$$

The system matrix $\boldsymbol{A}$ can be constructed by removing one block from the top and one block from the bottom of $\boldsymbol{\mathcal{O}}$. In the first block of $\boldsymbol{\mathcal{O}}$, the output matrix $\boldsymbol{C}$ can be found [7].

In contrast to BAYOMA, the elements of the mode shape vectors identified using SSI are complex-valued. In case of a modally damped system, the mode shape is therefore oriented in a straight line in the complex plane at an angle called mean phase (MP) [25]

$$\mathrm{MP}(\boldsymbol{\varphi}_j) = \arctan\left(\frac{-V_{12}}{V_{22}}\right) \text{ with } \boldsymbol{USV}^T = [\mathrm{Re}(\boldsymbol{\varphi}_j)\ \mathrm{Im}(\boldsymbol{\varphi}_j)], \tag{15}$$

where $\boldsymbol{USV}^T$ is the SVD. V_{12} as well as V_{22} are the corresponding elements of the matrix $\boldsymbol{V}$. Using the mean phase, the mode can then be rotated to the real axis accordingly

$$\boldsymbol{\varphi}_{j,real} = \mathrm{Re}\left(\boldsymbol{\varphi}_j e^{-i\,\mathrm{MP}}\right). \tag{16}$$

In this process, deviations from the mean phase lead to inaccuracies. The mean phase deviation (MPD) metric

$$\mathrm{MPD}(\boldsymbol{\varphi}_j) = \frac{\sum_{k=1}^{n} \left|\boldsymbol{\varphi}_{jk}\right| \arccos \left| \dfrac{\mathrm{Re}(\boldsymbol{\varphi}_{jk})V_{22} - \mathrm{Im}(\boldsymbol{\varphi}_{jk})V_{12}}{\left|\boldsymbol{\varphi}_{jk}\right|\sqrt{V_{12}^2 + V_{22}^2}} \right|}{\sum_{k=1}^{n} \left|\boldsymbol{\varphi}_{jk}\right|} \tag{17}$$

has been established as a quality criterion for identified mode shapes [25]. In Eq. 17, n is the number of elements of the mode shape $\boldsymbol{\varphi}_j$. Closely spaced modes can be detrimental to the mode shape identification and should be considered when using this established procedure. Further details are described in the next section.

2.3 Special aspects of closely spaced modes

There are several metrics for determining the closeness of natural frequencies [4, 30], which are mathematically similar. In this paper, the formulation by Au et al. [4] is chosen, because it is usually used in context of BAYOMA. The closeness of two modes can be expressed using the distance in terms of the frequency as well as the half-width of both modes. Therefore, in addition to the natural frequencies, the damping ratios are necessary to determine the closeness. For nearly equally damped modes, the close mode factor e_j for mode j can be calculated as follows

$$e_j = \left|\frac{f_k - f_j}{f_j \zeta_j}\right|. \tag{18}$$

In this study, the close mode factor e of a mode pair j and k is calculated as the mean value of e_j and e_k. A visualisation of the PSD of two modes with different close mode factors is shown in Fig. 2. For $e \leq 1$, the natural frequencies of the modes are within the half-power width of each other. This range is referred to as closely spaced modes in the following. From about $e > 10$ onwards, the modes are clearly

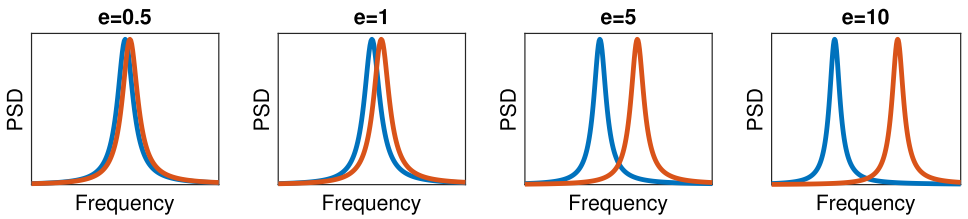

Fig. 2 A visualisation of the PSD of two modes with different close mode factors

well-separated. In the extreme case of two equal natural frequencies $e = 0$, a double eigenvalue problem occurs.

In this case, every linear combination of the two eigenvectors is also a eigenvector of the system, so that only the mode subspace (MSS) can be uniquely determined. A visualisation of the MSS for the first bending mode of a cantilever beam, spanned by the two linearly independent vectors $\boldsymbol{\psi}_k$ and $\boldsymbol{\psi}_m$ is given in Fig. 3. Another possible eigenvector is $\boldsymbol{\phi}_j$.

Usually, the frequencies are not exactly the same in real-world engineering structures. Theoretical considerations show that small mass and stiffness changes lead to rotations of mode shapes of very closely spaced modes within the MSS [8]. A more detailed investigation of the identification uncertainty of closely spaced modes demonstrates, that the mode shape in particular is more uncertain to identify than other modal parameters [4]. In case of a high signal to noise ratio (SNR) the identification of the MSS is possible with a very low uncertainty. The main part of the uncertainty of the mode shape is orthogonal to the MSS and corresponds to the position in the MSS. This uncertainty is independent of the SNR and depends mainly on the close mode factor e as well as the disparity factor d, which describes the ratio of the modal forces of the two modes

$$d_{jk} = \frac{S_{jj}}{S_{kk}}, \tag{19}$$

where S_{jj} is the modal force of the considered mode j and S_{kk} the modal force of the neighbouring mode k. The closer the modes and the smaller the disparity factor, the more uncertain is the position of the mode shape j in the MSS. For this reason, the well known modal assurance criterion (MAC) [1]

$$\mathrm{MAC}_{j,k} = \frac{\left|\boldsymbol{\varphi}_j^H \boldsymbol{\varphi}_k\right|^2}{\boldsymbol{\varphi}_j^H \boldsymbol{\varphi}_j \boldsymbol{\varphi}_k^H \boldsymbol{\varphi}_k}. \tag{20}$$

is prone to high uncertainties for closely spaced modes. Therefore, Gres et al. [17] propose to employ a scaled and shifted χ^2 distribution for the comparison of two almost equal modes considering their uncertainties. In the case of closely spaced modes, a beta distribution is better suited to describe the resulting probability density function [22].

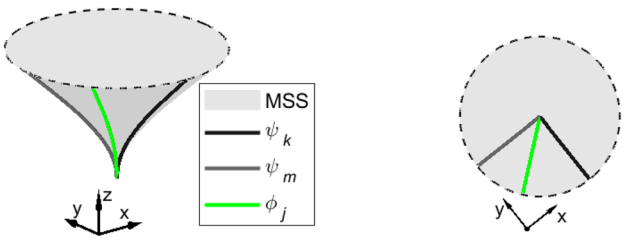

Fig. 3 Visualisation of the mode subspace (MSS) from the first bending mode pair $[\boldsymbol{\psi}_k \boldsymbol{\psi}_m]$ of a cantilever structure. Another possible mode shape $\boldsymbol{\phi}_j$ is shown in green (colour figure online)

A modification to MAC for comparing closely spaced modes is the subspace of order 2 modal assurance criterion (S2MAC) [13]. The S2MAC compares a subspace spanned by two mode shapes $[\boldsymbol{\psi}_k \boldsymbol{\psi}_m]$ with a mode shape vector $\boldsymbol{\varphi}_j$. For real-valued unit norm modes, such as those resulting from BAYOMA identification, the S2MAC can be calculated as

$$\mathrm{S2MAC}_{j,k,m} = \frac{(\boldsymbol{\varphi}_j^T \boldsymbol{\psi}_k)^2 - 2(\boldsymbol{\varphi}_j^T \boldsymbol{\psi}_k)(\boldsymbol{\psi}_k^T \boldsymbol{\psi}_m)(\boldsymbol{\varphi}_j^T \boldsymbol{\psi}_m) + (\boldsymbol{\varphi}_j^T \boldsymbol{\psi}_m)^2}{1 - (\boldsymbol{\psi}_k^T \boldsymbol{\psi}_m)^2}. \tag{21}$$

Similar to the distribution of the MAC, the distribution of the S2MAC can be expressed as a beta distribution.

In this paper a tower with closely spaced bending modes is examined. The vibration is measured in x- and y-direction in all measuring levels (ML). Accordingly, the direction angle γ of a mode shape can be calculated analogously to the MP in Eq. 15

$$\gamma = \arctan\left(\frac{-V_{12}}{V_{22}}\right) \text{ with } \boldsymbol{USV}^T = [\boldsymbol{\varphi}_x\ \boldsymbol{\varphi}_y], \tag{22}$$

where $\boldsymbol{\varphi}_x$ are the entries of the mode shape in x-direction, and $\boldsymbol{\varphi}_y$ are the entries of the mode shape in y-direction. For bending modes, the angle corresponds to the alignment of the mode shape in the MSS and is accordingly subject to higher uncertainty. The distribution of the direction angle can be modelled as a Gaussian distribution.

In order to compare the mode shapes identified with BAYOMA and SSI-COV, the complex mode shapes have to be transformed to real mode shapes. In the case of closely spaced modes, greater care is required. The mode shapes are often not on one straight line in the complex plane. In the case of a nearly axisymmetric structure, a circle was observed in the complex plane [15]. The measurement was taken at one height at six different angles in radial direction of the structure to investigate wineglass modes. To monitor bending modes, in many applications, two sensors are used at one height, which measure at 90° to each other. If measurements are situated at different heights, two dominant lines are observed—one for every measurement direction—in the complex plane for each mode shape in the case of closely spaced modes. This will be shown in more detail in Chapter 4.

When converting the mode into real space according to Eq. 16, this can lead to an incorrect alignment of the mode. As a result, the direction angle γ can be incorrect. When comparing with a mode subspace using the S2MAC, the error has no influence. One indicator of the phenomenon

is the MPD. When separate mean phases occur for each measured spatial direction the MPD increases.

3 Investigated structure

The experiment took place at the Test Centre Support Structures located at the Leibniz University of Hannover. The investigated prestressed reinforced concrete tower consists of 16 conical concrete ring segments (designated E1 to E16) with a total height of 7.5 m and is shown in Fig. 4.

Each individual segment has a wall thickness of 4 cm and a compressive strength of 7 7MPa. The lowest concrete ring is fixed to the foundation by a high-strength mortar. A steel cross serves as the upper tower termination, which is joined to the uppermost concrete ring segment by a steel insert. To preload the joints, a tendon is used in the tower centre, which is anchored to the foundation and to the head construction. In addition, the foundation is attached to the clamping field with four steel anchors. The pre-tension force applied is about 300 kN per steel anchor.

In this experiment, local joint monitoring at the lowest joint, as well as global monitoring of tower and tendon dynamics are investigated. Low-noise IEPE accelerometers with a customised IEPE signal conditioner with a high-pass filter cut-off frequency of 0.0106 Hz are used to measure the dynamics of the tower [21]. Two accelerometers are mounted on each concrete segment in the x and y-direction to investigate the bending modes of the tower (32 accelerometers in total).

To determine the preload, four electrical strain gauges are installed on the tendon on two measurement levels. Two strain gauges were installed at each level. In addition, three acceleration sensors are attached to the steel in x-direction to determine the natural frequencies of the tendon.

It is expected, that the highest imperfections of the surface of the dry joint can be observed between segment E16

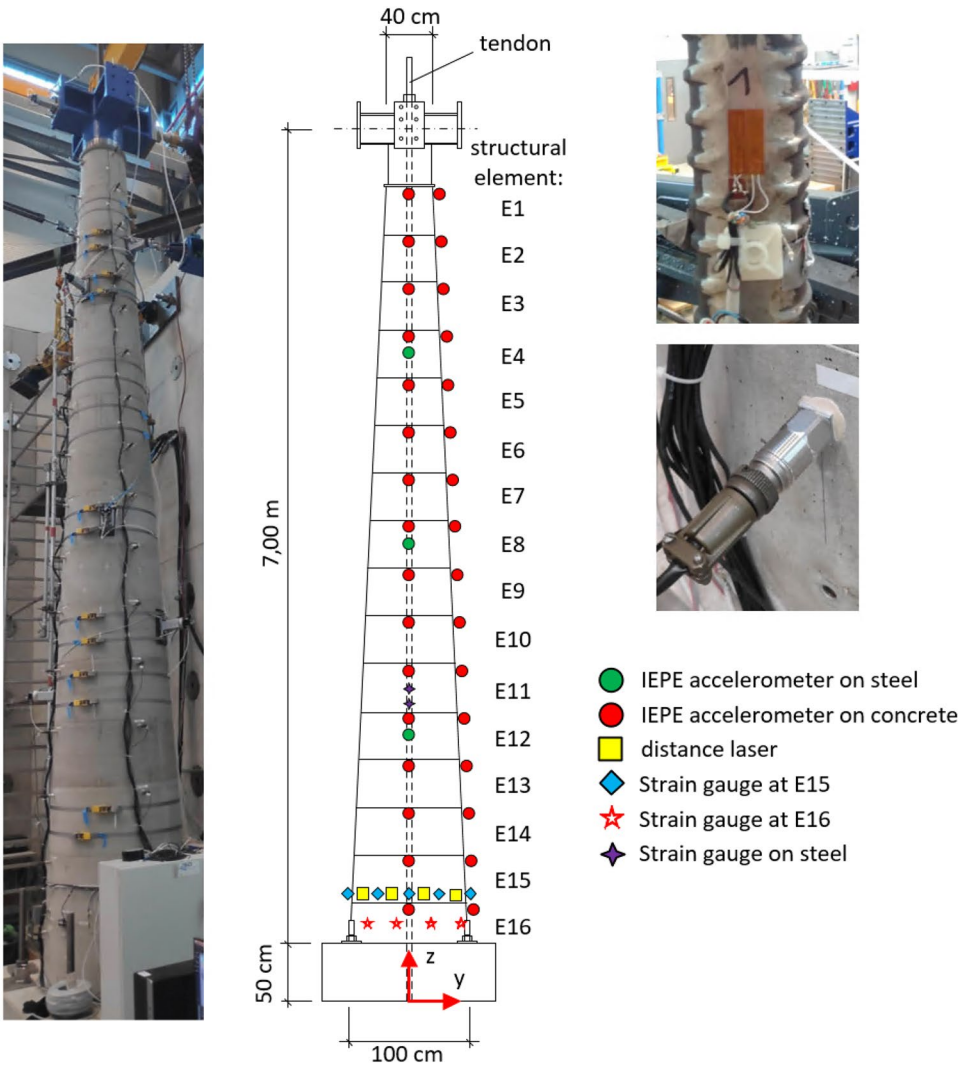

Fig. 4 Sensor setup attached to the tower. Left: Picture of the tower, center: sketch of the tower with measuring positions, top right: strain gauge on the tendon, center right: IEPE accelerometer

and E15 due to the largest joint surface. Therefore, sensors for local monitoring are installed at the lowest joint between segment E16 and E15. The changes in strain distribution in z-direction over the circumference of the ring segment are recorded by eight selectively arranging strain gauges placed in the immediate vicinity of the joint (blue diamonds in Fig. 5) as well as eight strain gauges at a distance of 20 m from the joint (red stars in Fig. 5). In addition, eight laser sensors distributed around the circumference above the strain gauges on segment E16 measure the change in displacement due to changing preload from 15 mm above to 15 mm below the joint. The detailed arrangement of the sensor setup at the segments E15/E16 is shown in Fig. 5. It should be noted that at segment E16, the strain gauge failed at 73 degrees.

4 Results

In this section, the influence of preload on the natural frequencies and mode shapes is investigated in more detail. In the following, a credible interval encompassing two standard deviations is used for the uncertainties of the natural frequencies and the direction angle in the figures. This corresponds approximately to a 95% credible interval, which is used to display MAC and S2MAC.

For each preload level, 40 data sets are evaluated. The number of data sets results from a data selection that excluded too strong harmonic disturbing excitation from the operation in the laboratory as well as a uniform size per preload. The measurement time for each data set is 10 min and the signals were recorded simultaneously using a sampling rate of 1000 Hz and a 24bit digital to analogue converter.

4.1 Influence of the preload on the joint

An important parameter for segmented towers is the preload. The preload F_p can be determined from the strain gauges on the tendon

$$F_p = \epsilon_{\text{meas}} E_{\text{steel}} A_{\text{steel}}, \tag{23}$$

where E_{steel} is the Young's modulus of steel, ϵ_{meas} is the measured strain on the tendon and A_{steel} is the effective cross-sectional area. The dependence of the strain on the preload close to the lowest joint and in the middle of the ring segment E16 is shown in Fig. 6.

The strain measurements, shown in Fig. 6a, imply that the load transfer between the joint starts at different preload levels at the different measurement points. This is indicative of unevenness in the joint and is consistent with the results of Klein et al. [23]. The expected linear relationship sets in at a preload level above 500 kN for all strain gauges. The strain distribution is more homogeneous in the middle of segment E16 (Fig. 6b), which is evident from a linear relationship between strain and preload at lower preload levels. Nevertheless, there are deviations in the strain distribution over the entire cross-section, which can be caused by an inhomogeneous material. In addition, it can also be the effect of the imperfection of the joint. In Fig. 6c, the laser measurements initially show large increase in displacement at low preloads, which changes to the expected linear relationship as the preload increases. The higher increase in displacement at low preload compared to higher preload mainly occurs due to the closing of the joint. At higher preload, the linear behaviour is caused mainly by the straining of the concrete. The deviations of the displacements, as well as the strain at the joint in Fig. 6a, over the cross-section indicate an imperfection of the joint due to a waviness. Thus, the strain and displacement sensors, which are mounted shifted by 22.5 degrees, do not show any similar trends in the distribution. The dynamics of the tower are studied at five preload levels (150 kN, 300 kN, 450 kN, 640 kN and 750 kN), which are

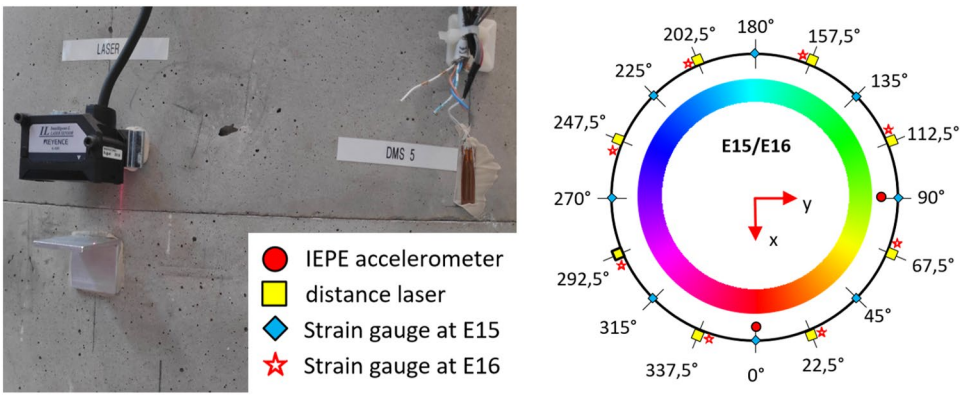

Fig. 5 Displacement laser sensors and strain gauges at the joint between segment E15 and E16. The colour gradient in the right shows the colours for the different sensor positions for Fig. 6 (colour figure online)

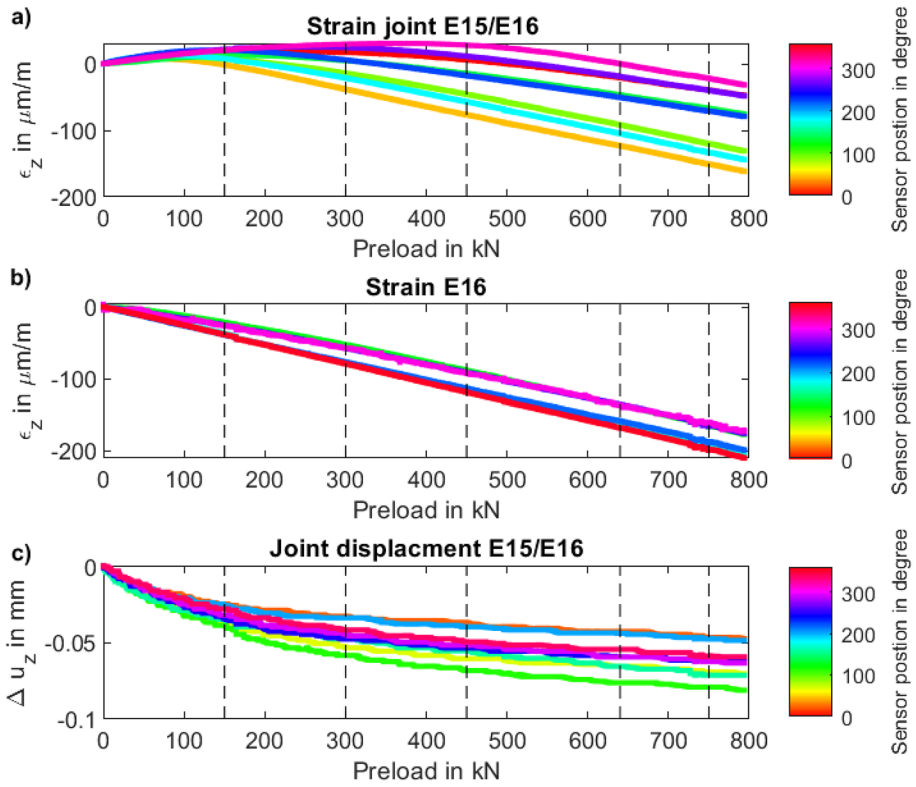

Fig. 6 Dependence of strain and displacement in z-direction on the preload

marked by the black dashed lines in Fig. 6. Due to the strain distribution at the joint shown in Fig. 6a as well as the displacement distribution shown in 6c, it can be assessed that only a part of the joint surface is involved in the load transfer at the lower three preload levels.

4.2 Influence of the preload on the dynamics of the tower

The basics of the dynamics of the tower are initially presented using the first preload level of 150 kN. For further investigations, all preload levels are used. The experiments are performed under ambient excitation, which is mainly caused by machine equipment operating in the laboratory. The upper part of Fig. 7 shows the first two singular values in the spectral matrix of the acceleration sensors in the frequency range from 0 Hz to 45 Hz. The averaged spectrum is not used for the identification but only for visualisation.

In the following, the first two bending mode pairs and the first tendon mode are evaluated. The ranges used for identification with BAYOMA are marked black in the upper diagram of Fig. 7. The frequency ranges between 15 Hz and 20 Hz, as well as 30 Hz and 35 Hz are not considered further, since they belong to modes where mainly the tendon is moving decoupled from the rest of the structure. If only accelerometers on the tower are used to calculate the averaged spectral matrix, the peaks between 15 and 20 Hz become significantly smaller as shown in the middle of Fig. 7. Nevertheless, the first tendon mode is still strongly excited. This is due to the interaction of the first tendon mode with the tower. The tendon accelerometers are not used to identified the bending modes of the tower in order to prevent unnecessary noise. The narrow peaks (e.g. between 24 and 26 Hz) in the spectrum are caused by harmonic excitation from aggregates located in the laboratory. In order to save computing time, especially when using the SSI, the signals are low-pass filtered and subsequently downsampled to 125 Hz, as the modes investigated in this study are below 50 Hz. For identification using the SSI, model orders up to 120 are evaluated. The covariance matrices are formed from the inverse DFT of the spectral matrices. Since BAYOMA always uses an unaveraged spectrum for the identification, the SSI is applied in the same manner. The mode selection of the SSI is done by a multi-stage clustering algorithm [25], which takes eigenvalue, frequency and damping deviation as well as the MAC as criteria. In contrast to [25] the MPD is not used as a criterion, because of the mean phases divided according to the measurement direction. An example of a stabilisation diagram is shown in the lower diagram of Fig. 7, where the modes are marked according to the clustering results. In Fig. 8, the two investigated bending mode shapes of the tower with dominant x-direction for a preload of 150 kN identified with BAYOMA are shown. The mode shapes of the SSI are similar and therefor not shown.

The tendon mode is not shown in this figure due to the low spatial sensor resolution on the tendon.

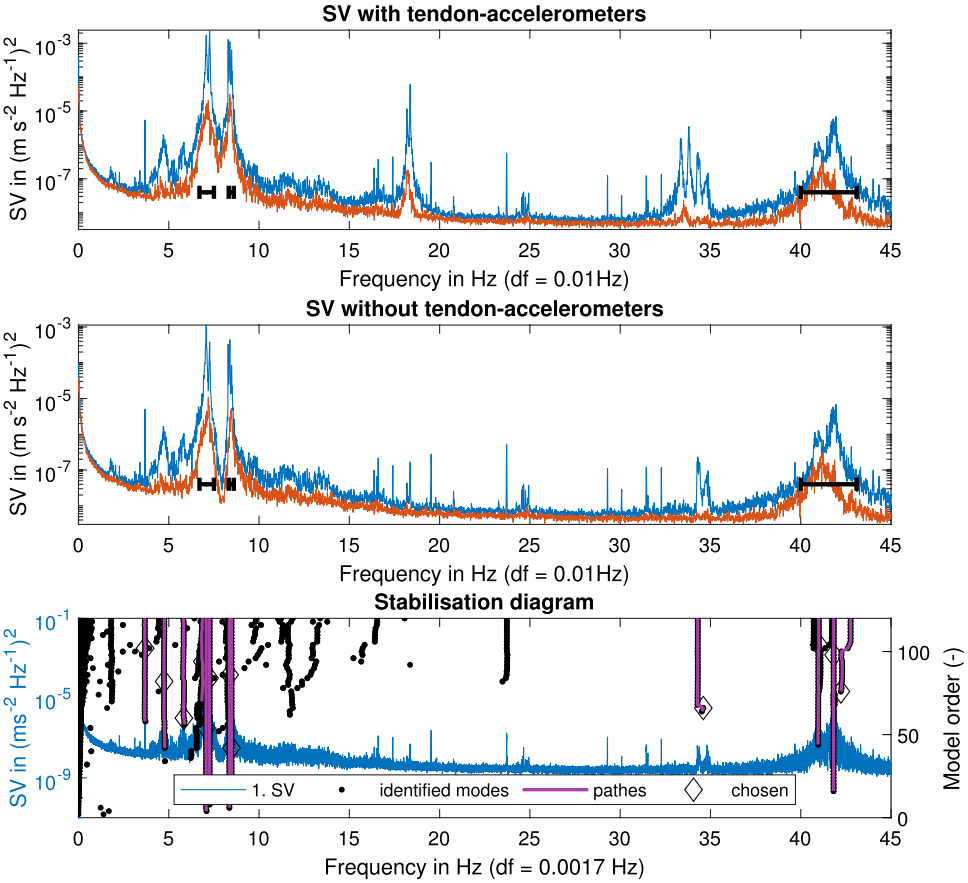

Fig. 7 Top: Two highest singular values (SV) of the averaged spectral matrix with tendon-accelerometers. The identification range of BAYOMA is marked with black lines. Middle: Without tendon-accelerometers. Bottom: Stabilisation diagram from the SSI-COV based on an unaveraged spectral matrix. The data is from a measurement at a preload level of 150 kN

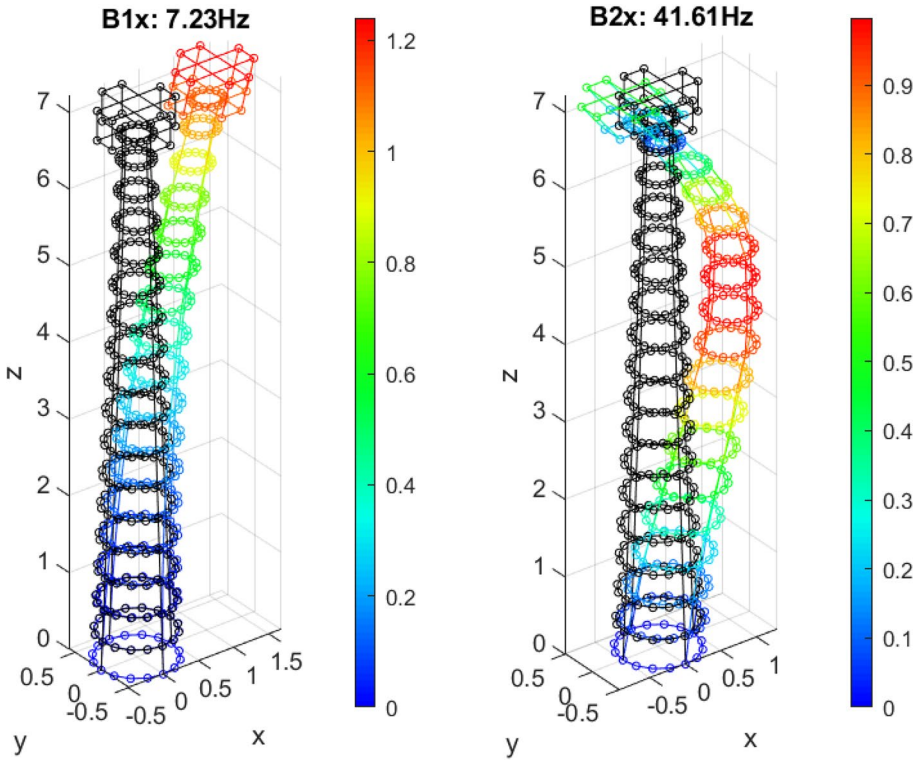

Fig. 8 Mode shape of the first two bending modes in the *x*-direction at 150 kN preload identified with BAYOMA. For visualisation, a linear interpolation is used between the sensors and outside the sensors a linear extrapolation. The deflection in the clamping is set to 0

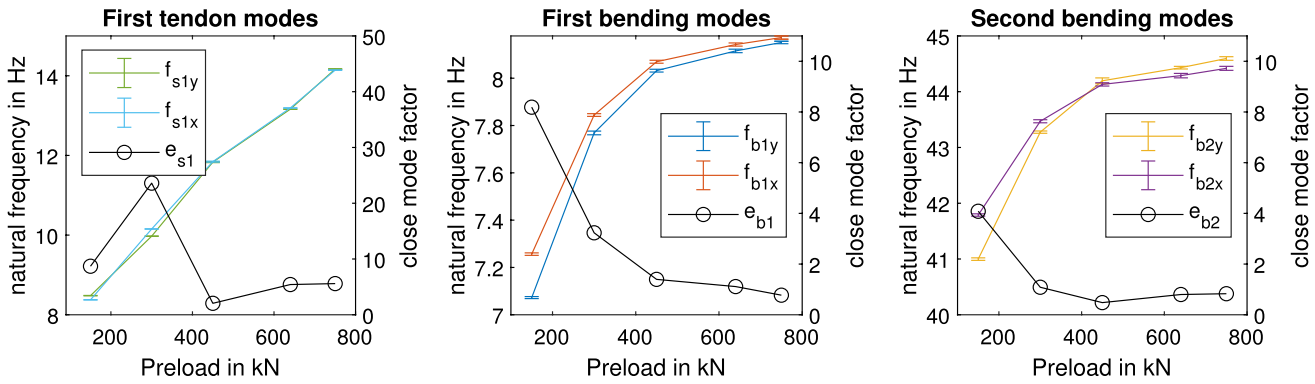

Fig. 9 The averaged and the 95% confidence interval of the natural frequencies identified with BAYOMA and the close mode factor as a dependence on the preload levels

The influence of the preload on the investigated natural frequencies is shown in Fig. 9. As expected, there is an almost linear relationship between the preload and the first tendon mode. Thus, the imperfections have only a minor influence on the tendon mode, so the modes will not be considered further in the investigations. The situation is different for the bending modes of the tower structure. At the low preload level, the bending modes are each well separated in the frequency domain. As the preload increases, the distance in the frequency domain between the bending modes decreases. In addition, all natural frequencies increase. This effect decreases with higher preload levels. The cause of this effect is probably the imperfections in the joints. With low preload, only parts of the joint surface participate in the load transfer, which leads to an asymmetric stiffness in the bending directions. As the preload increases, a larger area contributes to the load transfer so that the stiffness becomes more symmetrical. Therefore the natural frequencies are getting closer. Due to this effect, it becomes possible to investigate the influence of closely spaced modes on the same structure for different distances in the frequency range. Unlike the first pair of bending modes, the closeness of the second bending modes increases up to a preload of 450kN and then decreases slightly. This may be due to imperfections, but cannot be said with absolute certainty. A comparison of the two applied identification methods using the B1X mode as an example is shown in Fig. 10.

The natural frequencies are normalised for each preload level to the median of the natural frequency identified with BAYOMA. The deviation of both identification methods is less than 0.5 % for all preload levels. Noticeable are the deviations of the lowest preload level. However, these are negligible compared to the system change. Basically, both identification methods identify similar natural frequencies, which correspond to the trend of Fig. 9, so the observed effect in natural frequencies does not depend on the identification method.

In the following, the mode shapes are examined in more detail. For this study, the MAC, S2MAC and the direction angle γ identified with BAYOMA are used. The most probable value (MPV) and the uncertainty of the parameters are determined from the covariance matrices of the mode shape using a Monte Carlo method with 1000 samples each. A beta distribution is assumed for the MAC and S2MAC, while a normal distribution is used for the direction angle. The

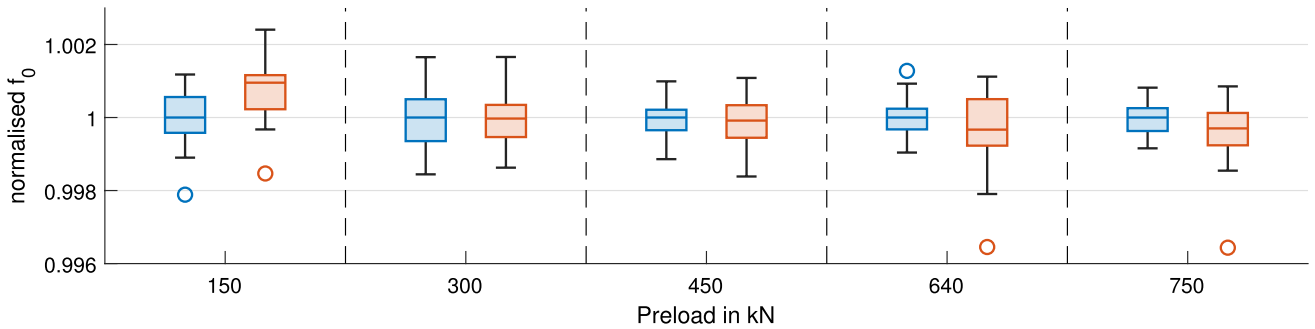

Fig. 10 Comparison of B1X natural frequency identified with BAYOMA (blue) and SSI-COV (red). For normalisation, the median of the natural frequency identified with BAYOMA is used for each preload level (colour figure online)

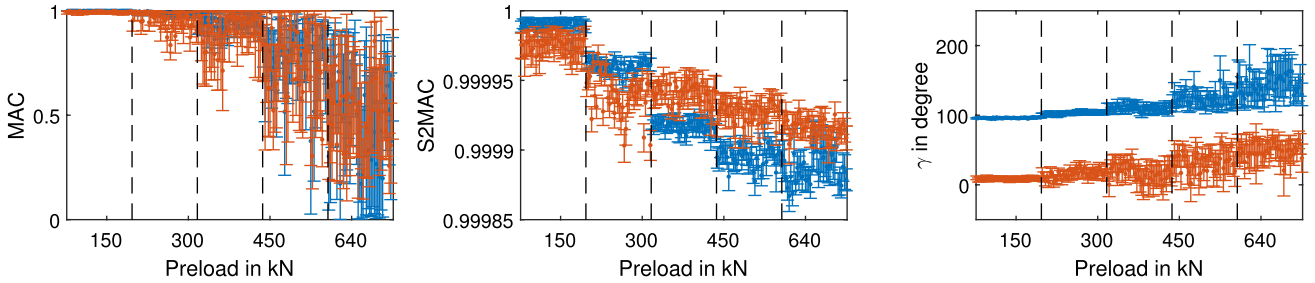

Fig. 11 Influence of the preload on the MAC, S2MAC and direction angle γ of the first bending mode pair identified with BAYOMA. Red is the B1X, blue the B1Y (colour figure online)

identification results of the first measurement at a preload level of 150 kN serve as the reference mode shapes.

Figure 11 shows the MAC, S2MAC and direction angle for the first bending mode pair. As expected, the uncertainty of the MAC as well as of the direction angle increases with decreasing distance in the frequency domain and thus increasing preload. However, the uncertainty of the S2MAC stays nearly constant, while the absolute value decreases slightly. This indicates a minor change in the MSS, which is slightly larger in the B1Y direction. This observation supports the theory, that the MSS of closely spaced modes remains relatively constant for small system changes and the main change is in the alignment of the mode in the MSS. Since the S2MAC only indicates changes in the MSS, it remains close to 1. The MAC compares two mode shapes so that changes in alignment are also noticeable in the MAC. The results of the modes identified with the SSI are very similar, so they are not presented.

The most significant changes of the mode shape at different preload levels is the direction angle γ. The trend of that angle of the mode shape identified with BAYOMA and the SSI is shown in Fig. 12.

As the preload increases, the mode rotates slightly counterclockwise independent of the identification method. This supports the theoretical considerations of Brincker et al. [8], which state that a rotation of the mode shapes in the MSS is observed in the transition from well-separated modes to closely spaced ones. In this experiment the direction angle is nearly equivalent to the rotation angle in the MSS. It is also apparent, that the observed uncertainties are increasing.

Similar results were obtained for the second bending mode pair, as shown in Fig. 13.

The smaller the distance in frequency space, the lower the MPV of the MAC value. Also, the uncertainties of the MAC as well as of the direction angles increase the closer the modes become. In contrast to the first pair of bending modes, the B2X mode is identified more reliably except for a preload of 450 kN. At this preload level, the MAC and direction angle scatters very strongly, because in this case, the modes are very closely spaced. Like the first bending mode

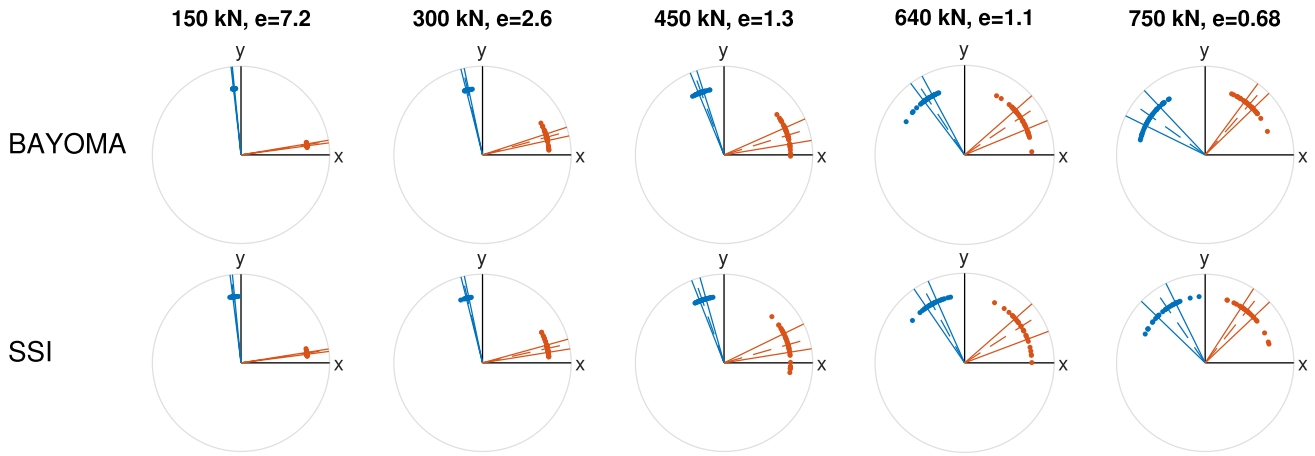

Fig. 12 Direction angle γ of the first bending mode pair at different preload levels with the median of the corresponding close mode factors e calculated from BAYOMA identifications. Dots are single measured values, lines correspond to the 25-75 percent percentile and the dashed line to the median. Red is the B1X, blue the B1Y. The upper line represents the identification with BAYOMA, the lower with the SSI (colour figure online)

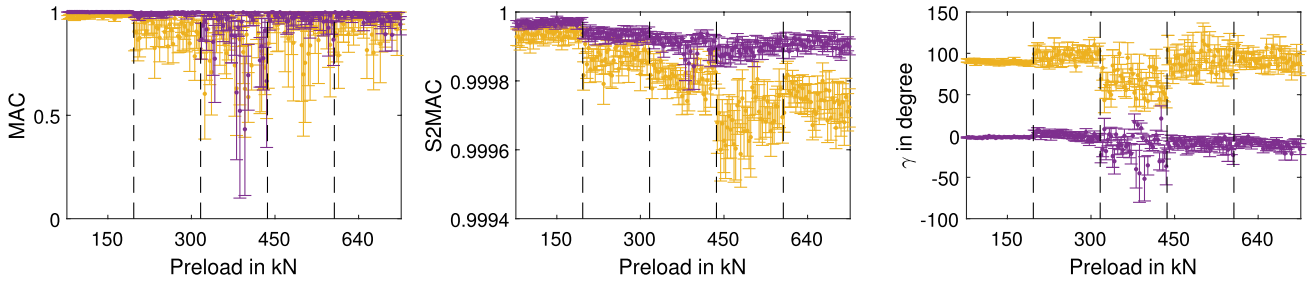

Fig. 13 Influence of the preload on the MAC, S2MAC and direction angle γ of the second bending mode pair identified using BAYOMA. Purple is the B2X, yellow the B2Y

pair, the bending mode in y-direction deviates more from the reference MSS than the one in x-direction, which can be observed with the S2MAC and indicates a change of the MSS. Due to the change of the MSS compared to the reference MSS at 150kN, a part of the high alignment uncertainty also affects the S2MAC. Thus, the S2MAC becomes more uncertain with increasing preload.

As with the first bending mode pair, mode rotation can be observed by changing the preload, which is shown in Fig. 14. In addition, a greater scattering is also observed for closer modes. In this case, the observed clockwise rotation of the alignment of the mode correlates with the close mode factor. For higher preload levels, the median of the direction angles differs between the two identification algorithms for both bending mode pairs. Possible reasons are the lower energy level at higher preload levels and the errors during the transformation of complex modes of the SSI to real ones due to multiple dominant phases in the complex plane.

Figure 15 shows that the uncertainty of the direction angle is mainly dependent on the close mode factor. With a decreasing close mode factor, the standard deviation of the alignment angle increases. For the second bending mode pair, in contrast to the first bending mode pair, a linear trend appears to be present in the logarithmic representation, which is only absent at the 450kN preload level due to the large scattering. The cause of the scattering is probably due to the very closely spaced modes. The standard deviation of the first bending mode dominating in the x-direction is significantly higher than in the y-direction except at 750kN preload. For the second pair of bending modes, the standard deviation of the B2Y mode is higher than the one of the B2X mode. This is consistent with the investigation in Fig. 12 and Fig. 14. Au et al. [4] list in their proposed uncertainty laws for closely spaced modes further influences on the uncertainty of the mode shape within the mode subspace, e.g. the ratio between the modal power of both modes, modal damping, and the number of periods in the measurement time. For latter reason, the angles of the second bending mode pairs can be determined with less uncertainty than those of the first mode. The difference in the uncertainties of the x

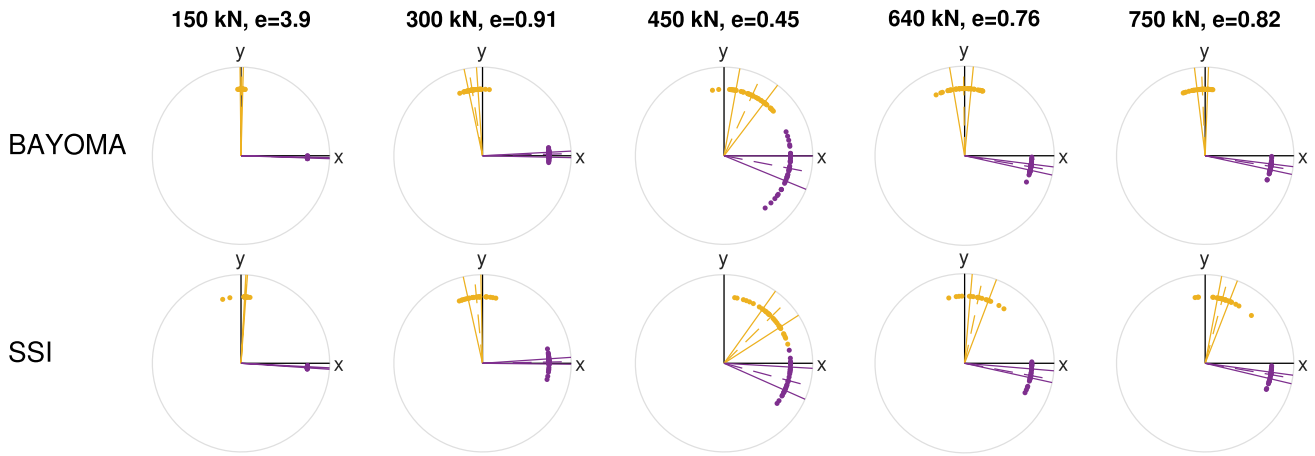

Fig. 14 Direction angle γ of the second bending mode pair at different preload levels with the median of the the corresponding close mode factors e calculated from BAYOMA identifications. Dots are single measured values, lines correspond to the 25-75 percent percentile and the dashed line to the median. Purple is the B2X, yellow the B2Y. The upper line represents the identification with BAYOMA, the lower with the SSI (colour figure online)

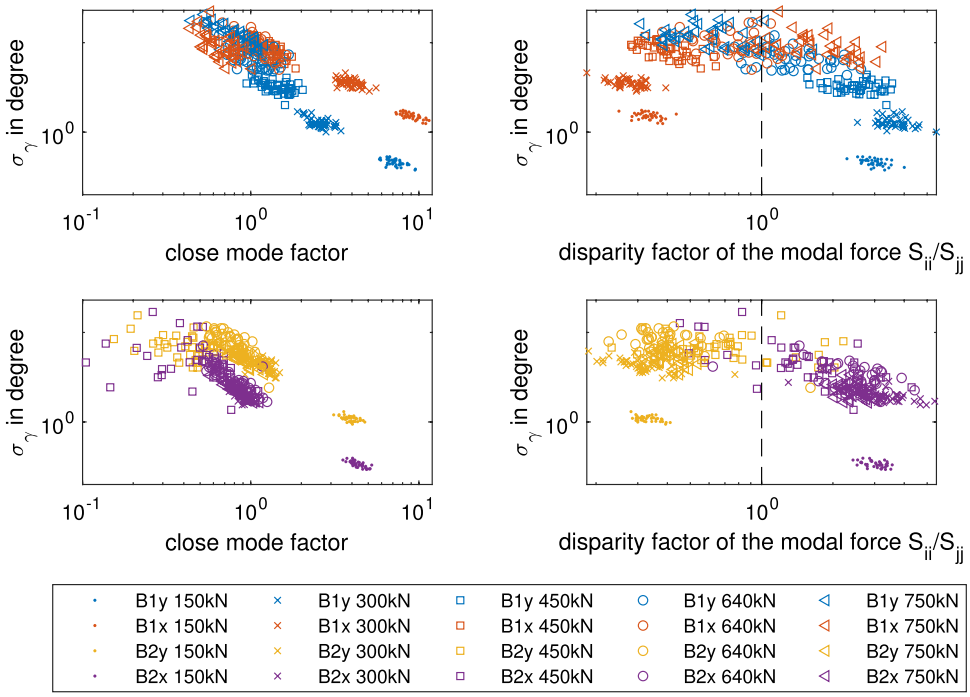

Fig. 15 Standard deviation of the direction angle γ of the mode shape as a dependence of the close mode factor e and the disparity factor d on the modal forces subdivided according to the different preload levels

and y-direction occurs due to the different excitation levels. The more excited mode with a disparity factor greater than 1 has a lower standard deviation of the direction angle than the less excited mode. For this reason, at 750kN the higher alignment angle uncertainty changes from B1x to B1y mode. Without the change of the disparity factor, the close-mode factor would be linearly related to the angular uncertainty in the double logarithmic representation, as in the second bending mode pair. It is important to note that the signal to noise ratio has no influence on the uncertainty of the mode alignment in the mode subspace, but on the identification of the mode subspace itself [4].

Theoretically, the identification uncertainty of BAYOMA should be similar to the observed uncertainty if all assumptions are satisfied and the data sets are comparable [2]. However, despite of laboratory conditions, there are differences in the data sets, such as excitation and small temperature changes, so that the observed and identification uncertainty of BAYOMA differ. A comparison of the uncertainty of the direction angle is shown in Fig. 16.

Here, the boxplots correspond to the identification uncertainty of BAYOMA of the individual measurement data sets. The observed standard deviation of the entire measurement series of the MPV of BAYOMA is shown in green and of the SSI in magenta. The trend of the observed and identification uncertainties is the same for the studied modes. However, the observed uncertainties are often higher. Particularly large deviations of the uncertainties

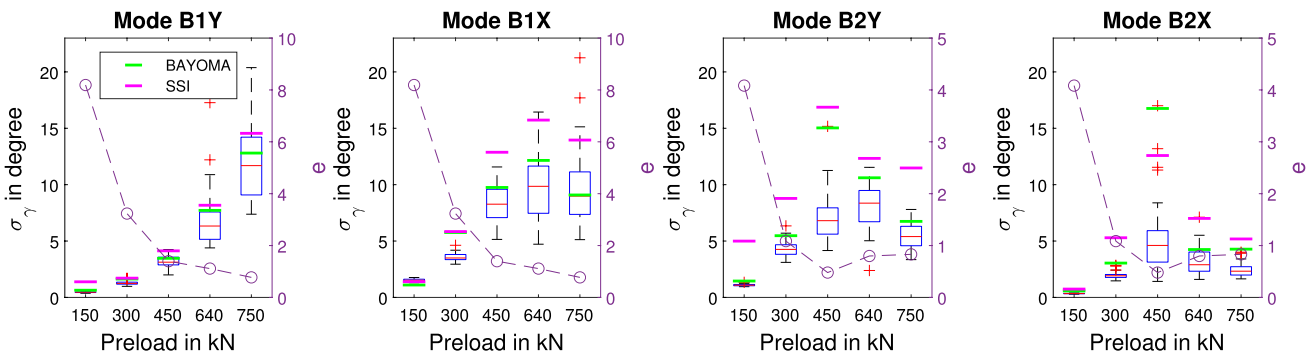

Fig. 16 Comparison of the identification uncertainty of BAYOMA (boxplot) and the observed uncertainty (BAYOMA: green line, SSI: magenta line) of the direction angle γ for different preload levels. The close mode factor e of identification results of BAYOMA is shown as well (colour figure online)

can be observed for lower close mode factors. The reasons are temperature as well as excitation changes in the period under consideration. In addition, assumptions of BAYOMA, especially of the excitation, may be violated, so that the calculated uncertainties may be inaccurate. Moreover, the observed uncertainty of the angle of the SSI is mostly higher than the one of BAYOMA. The reason for the higher dispersion is probably the effect of the two mean phases of the complex mode shape in the complex plane separated by the measurement directions, as shown in Fig. 17.

A real mode is necessary for the calculation of the direction angle. Due to the two dominant phases in the complex plane, an error occurs in the transformation from the complex to the real mode, which is noticeable in the alignment of the mode. A measure for the inaccuracy is the mean phase deviation (MPD), which is shown for the four observed modes in Fig. 18.

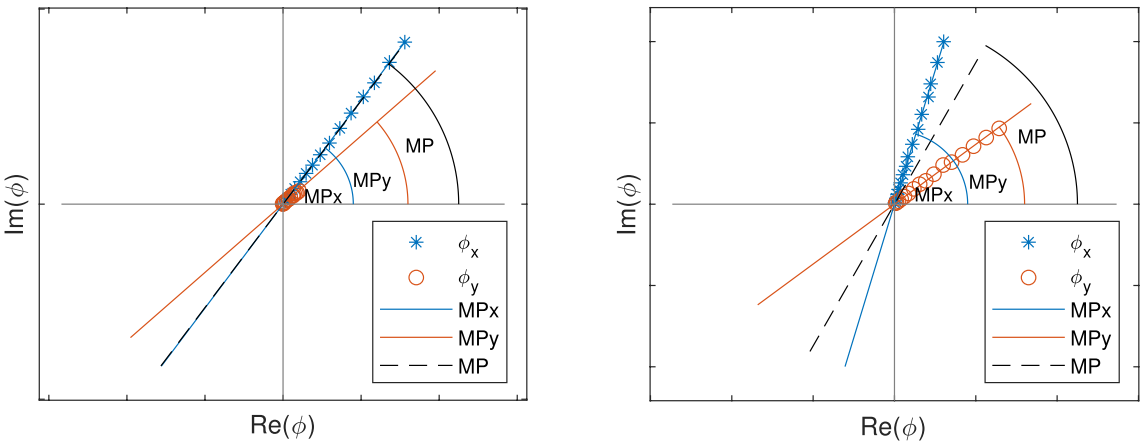

Fig. 17 Illustration of two B1X modes of two different preload levels in the complex plane separated according to measurement directions. On the left for a mode at a preload level of 150 kN, that the MP is almost identical to the MP in the dominant direction. On the right for a mode at a preload level of 750 kN, where two lines exist in the complex plane

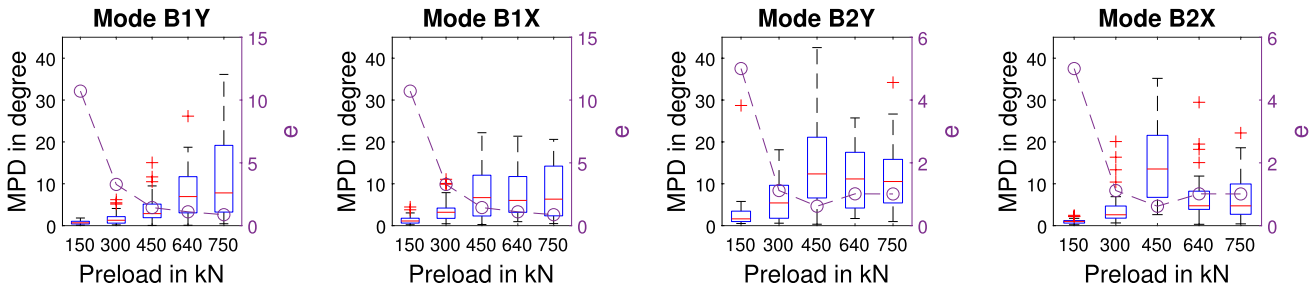

Fig. 18 Distribution of the MPD of the complex mode shape of the SSI as well as the close mode factor e as a function of the preload levels

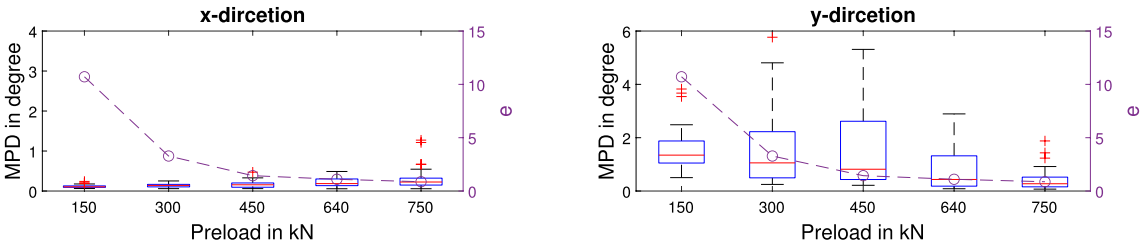

Fig. 19 Distribution of the MPD of the complex mode shape B1X of the SSI as well as the close mode factor e as a function of the preload levels separated according to measurement directions

As expected the MPD values correlate with the close mode factor. As shown in Fig. 17, at higher preload levels each measurement direction has a different mean phase in the complex plane. This leads to high MPD values and errors in the transformation into the real space. By taking into account the measurement directions separately, the MPD becomes significantly lower. This is shown in Fig. 19 for the B1X mode.

The MPD values in the dominant x-direction is significantly lower, which supports the hypothesis of two different phases in the complex plane.

5 Summary and outlook

This study investigates the influence of small system changes on the modal parameters of a large-scale experimental prestressed concrete tower with a total height of 7.5 m. The system changes are introduced by changing the preload, which changes the influence of the imperfections due to surface waviness of dry horizontal joints. To monitor the effects of the imperfections at the joints, a local instrumentation encompassing strain gauges and laser sensors was applied to the lowest joint. With increasing preload, a larger area of the joint surface is likely to contribute to the load transfer. For both bending mode pairs, the respective distance between the natural frequencies becomes smaller with increasing preload. This effect makes it possible to experimentally investigate the influences of closely spaced modes in more detail for the same structure. The known effect that closer natural frequencies lead to a rotation of the mode shape in the mode subspace could be demonstrated experimentally using BAYOMA and SSI-COV. Furthermore, it could be shown that the uncertainty of the alignment of the mode shape in the MSS increases with the closeness of the modes. Another influence on the uncertainty is the disparity of the modal force of the closely spaced modes, which makes the alignment of the more excited mode significantly more reliable to identify. The S2MAC metric, which specifically indicates changes of the mode subspace, was found to be a more reliable quantity than the traditional MAC metric. Even a slight change in the mode subspace due to the preload change could be observed using the former metric. A comparison of the observed and identification uncertainty of BAYOMA of the direction angle shows that while the trend matches, significant deviations occurred in some cases. This can be explained on one hand due to changes in excitation, temperature, etc., which make the data sets not exactly comparable. On the other hand, BAYOMA's assumptions are almost always violated in reality, so the uncertainties are a good guide, but one should be aware that they are not numerically exact. The investigation of the complex mode shapes of closely spaced modes identified with the SSI-COV indicated different dominating phases in the complex plane separated by the measurement directions. This means that greater caution is required when transforming complex closely spaced modes into the real space. This may lead to higher uncertainties in the alignment of the real mode in the mode subspace compared to BAYOMA as shown in Fig. 16.

The study showed that for structures, which exhibit closely spaced modes as well as joints, the joint surface imperfections can have a great influence on the modal parameters - and here in particular - on the alignment of the mode shape in the mode subspace. It can therefore be assumed that other types of small system changes have a similarly significant effect on the mode shapes, but not necessarily on the natural frequencies. For this reason, methods based solely on tracking changes in natural frequencies or which use, e. g. overall vibration levels, may not be adequate to detect small system changes or damages. This should be the subject of future scientific research. In addition, methods that have modal parameters as input, like model updating for damage localisation, should take into account the imperfections. Furthermore, metrics should be used that are insensitive to the slight changes in mode alignment in the MSS. In the future, the influence of the imperfections of real wind turbine hybrid towers should be investigated. Moreover, appropriate data normalisation methods should be applied in order to reduce the influence of the imperfections and environmental and operational conditions, thereby enabling a reliable damage detection.

In future works on the experiment, the higher modes could be analysed using additional excitation sources. In addition, the identification uncertainties of the SSI [14] should also be calculated and compared with those of BAYOMA, especially for closely spaced modes. The cause of the different mean phases of the complex mode shape of closely space modes separated by measurement direction identified with the SSI, should also be investigated in more detail. The experiment will be used in the future to investigate the dynamic joint opening with a hydraulic actuator.

Acknowledgements We greatly acknowledge the financial support of the German Research Foundation (CRC 1463, subproject C02), the Federal Ministry for Economic Affairs and Energy of Germany (research projects *Deutsche Forschungsplattform für Windenergie*, FKZ 0325936E and *HyTowering - Optimierung der Bemessung hybrider Türme und Entwicklung eines geeigneten Monitoringkonzepts zur Schadensdetektion und -quantifizierung*, FKZ 0324221A) and the project partner Max Boegl that enabled this work.

Funding Open Access funding enabled and organized by Projekt DEAL.

Data availability The measurement data used in this work is published as an open-access data publication within the Research Data Repository of the Leibniz University Hanover that issues datasets with DOIs: https://doi.org/10.25835/d58o1q96.

Declarations

Conflict of interest The authors declare no potential conflict of interests.

References

1. Allemang RJ, Brown DL (1982) A correlation coefficient for modal vector analysis. Proceedings of the 1st International Modal Analysis Conference, Orlando: Union College Press **1**, 110–116
2. Au SK (2012) Connecting bayesian and frequentist quantification of parameter uncertainty in system identification. Mechanical Systems and Signal Processing 29:328–342. https://doi.org/10.1016/j.ymssp.2012.01.010
3. Au SK (2012) Fast bayesian ambient modal identification in the frequency domain, part i: Posterior most probable value. Mechanical Systems and Signal Processing 26:60–75. https://doi.org/10.1016/j.ymssp.2011.06.017
4. Au SK, Brownjohn JM, Li B, Raby A (2021) Understanding and managing identification uncertainty of close modes in operational modal analysis. Mechanical Systems and Signal Processing 147:107018. https://doi.org/10.1016/j.ymssp.2020.107018
5. Au SK, Zhang FL, Ni YC (2013) Bayesian operational modal analysis: Theory, computation, practice. Computers & Structures 126:3–14. https://doi.org/10.1016/j.compstruc.2012.12.015
6. Bögl S, Gläser C, Hierl M, Traute M (2013) Vorgespannte Hybridtürme für Windenergieanlagen. Bauingenieur 88(8):301–306
7. Brincker R, Andersen P (2006) Understanding stochastic subspace identification. In: Conference Proceedings: IMAC-XXIV: A Conference & Exposition on Structural Dynamics. Society for Experimental Mechanics
8. Brincker R, Lopez-Aenlle M (2015) Mode shape sensitivity of two closely spaced eigenvalues. Journal of Sound and Vibration 334:377–387. https://doi.org/10.1016/j.jsv.2014.08.015
9. Brincker R, Ventura C (2015) Introduction to operational modal analysis. John Wiley & Sons
10. Brincker R, Zhang L, Andersen P (2001) Modal identification of output-only systems using frequency domain decomposition. Smart Materials and Structures 10(3):441–445
11. Brownjohn JMW, Raby A, Au SK, Zhu Z, Wang X, Antonini A, Pappas A, D'Ayala D (2019) Bayesian operational modal analysis of offshore rock lighthouses: Close modes, alignment, symmetry and uncertainty. Mechanical Systems and Signal Processing 133:106306. https://doi.org/10.1016/j.ymssp.2019.106306
12. Camargo EA, Ulfkjaer JP, Brincker R, Nøergaard J, Gadegaard SS (2019) Operational modal analysis and finite-element model updating of pilot concrete wind turbine tower. Journal of Structural Engineering 145(2):05018003. https://doi.org/10.1061/(ASCE)ST.1943-541X.0002242
13. D'Ambrogio W, Fregolent A (2003) Higher-order mac for the correlation of close and multiple modes. Mechanical Systems and Signal Processing 17(3):599–610. https://doi.org/10.1006/mssp.2002.1468
14. Döhler M, Mevel L (2013) Efficient multi-order uncertainty computation for stochastic subspace identification. Mechanical Systems and Signal Processing 38(2):346–366. https://doi.org/10.1016/j.ymssp.2013.01.012
15. Dooms D, Degrande G, de Roeck G, Reynders E (2006) Finite element modelling of a silo based on experimental modal analysis. Engineering Structures 28(4):532–542. https://doi.org/10.1016/j.engstruct.2005.09.008
16. Farrar CR, Worden K (2012) Structural health monitoring: a machine learning perspective. John Wiley & Sons
17. Greś S, Döhler M, Mevel L (2021) Uncertainty quantification of the modal assurance criterion in operational modal analysis. Mechanical Systems and Signal Processing 152(8):107457. https://doi.org/10.1016/j.ymssp.2020.107457
18. Häckell MW, Rolfes R (2013) Monitoring a 5mw offshore wind energy converter–condition parameters and triangulation based extraction of modal parameters. Mechanical Systems and Signal Processing 40(1):322–343. https://doi.org/10.1016/j.ymssp.2013.04.004
19. Hosseini Kordkheili SA, Momeni Massouleh SH, Hajirezayi S, Bahai H (2018) Experimental identification of closely spaced modes using next-era. Journal of Sound and Vibration 412(12):116–129. https://doi.org/10.1016/j.jsv.2017.09.038
20. Jimenez Capilla JA, Au SK, Brownjohn JMW, Hudson E (2021) Ambient vibration testing and operational modal analysis of monopole telecoms structures. Journal of Civil Structural Health Monitoring 11(4):1077–1091. https://doi.org/10.1007/s13349-021-00499-4
21. Jonscher C, Hofmeister B, Grießmann T, Rolfes R (2022) Very low frequency IEPE accelerometer calibration and application to a wind energy structure. Wind Energy Science 7(3):1053–1067. https://doi.org/10.5194/wes-7-1053-2022
22. Jonscher C, Hofmeister B, Grießmann T, Rolfes R (2023) Influence of environmental conditions and damage on closely spaced modes. In: Rizzo, P., Milazzo, A. (eds.) European Workshop on Structural Health Monitoring, Springer eBook Collection, vol. 270, pp. 902–911. Springer International Publishing and Imprint Springer, Cham. https://doi.org/10.1007/978-3-031-07322-9_91
23. Klein F, Fürll F, Betz T, Marx S (2022) Experimental study on the joint bearing behavior of segmented tower structures subjected to normal and bending shear loads. Structural Concrete 23(3):1370–1384. https://doi.org/10.1002/suco.202100710
24. Peeters B, Van der Auweraer H, et al (2005) PolyMAX: a revolution in operational modal analysis. In: Proceedings of the 1st International Operational Modal Analysis Conference, Copenhagen, Denmark. vol. 820, pp. 1–12
25. Reynders E, Houbrechts J, de Roeck G (2012) Fully automated (operational) modal analysis. Mechanical Systems and Signal Processing 29(5):228–250. https://doi.org/10.1016/j.ymssp.2012.01.007
26. Reynders E, Maes K, Lombaert G, de Roeck G (2016) Uncertainty quantification in operational modal analysis with stochastic subspace identification: Validation and applications. Mechanical Systems and Signal Processing 66–67(4):13–30. https://doi.org/10.1016/j.ymssp.2015.04.018
27. Reynders E, Pintelon R, de Roeck G (2008) Uncertainty bounds on modal parameters obtained from stochastic subspace identification. Mechanical Systems and Signal Processing 22(4):948–969. https://doi.org/10.1016/j.ymssp.2007.10.009
28. Theiler W, Reicht O, Tue NV (2015) Auswirkungen von Unebenheiten bei trockenen Druckverbindungen von Betonbauteilen.

Beton- und Stahlbetonbau 110(10):687–698. https://doi.org/10.1002/best.201500003
29. van Overschee P, de Moor B (1993) Subspace algorithms for the stochastic identification problem. Automatica 29(3):649–660. https://doi.org/10.1016/0005-1098(93)90061-W
30. Woodhouse J (1998) Linear damping models for structural vibration. Journal of Sound and Vibration 215(3):547–569. https://doi.org/10.1006/jsvi.1998.1709
31. Yuen KV, Katafygiotis LS (2003) Bayesian fast fourier transform approach for modal updating using ambient data. Advances in Structural Engineering 6(2):81–95. https://doi.org/10.1260/136943303769013183